Explicit Dynamic Finite Element Simulation of Plate Impacts for Damage Localisation

Luke Pollock, Noemi North, and Graham Wild

Abstract: This work explores the application of the explicit dynamic Finite Element Analysis (FEA) software, LS-DYNA for the simulation of low velocity impacts upon metallic plates as a preliminary assessment for similar work in Fiber Reinforced Polymers (FRPs). Impacts are performed on a flat (100 x 100) mm aluminium plate of 1 mm thickness using a 10 mm spherical steel projectile. Impact events between 2.5 J and 20 J are performed and the acoustic and modal response of the plate is analyzed. The aim of this work is to provide a framework that would allow for the localization and interrogation of impact events for the assessment of Barely Visible Impact Damage (BVID) in FRPs. The challenges of BVID are discussed as well as the future work to be undertaken towards the development of an Acoustic Emission (AE) Structural Health Monitoring (SHM) system.

Keywords: Finite element, Acoustic emissions, Low velocity, BVID, FRP, Composites

Nomenclature

FEA	:	Finite Element Analysis
AEs	:	Acoustic Emissions
FRPs	:	Fibre Reinforced Polymers
BVID	:	Barely Visible Impact Damage
NDT	:	Non-Destructive Testing
SHM	:	Structural Health Monitoring
CFL	:	Courant-Friederich Levy

1. Introduction

The aim of this work is to examine the potential application of explicit dynamic Finite Element Analysis (FEA) simulations using the software package LS-DYNA for the interrogation of Acoustic Emissions (AEs) released from low velocity impacts for the purposes of acoustic source localization. Low velocity impacts most commonly occur in aerospace structures from tool drops, runway debris (Kumar and Rai, 1993) or in-flight debris such as hail (Fawcett and Oakes, 2006) and can have severe effects upon the mechanical performance of Fiber Reinforced Polymers (FRPs) (Mustapha et al., 2016, Saeedifar et al., 2018).

Fig. 1 A depiction of the mechanisms behind the formation of BVID resulting from low-velocity impacts in FRPs (Azouaoui, Azari, & Pluvinage, 2010).

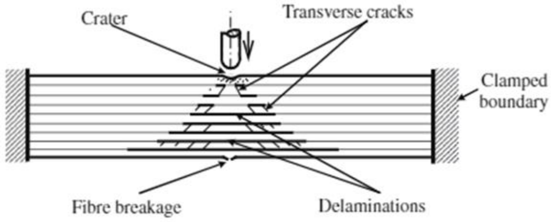

The possible result of a low velocity impact is the formation of Barely Visible Impact Damage (BVID) that can be difficult to detect in visual inspections, requiring advanced Non-Destructive Testing (NDT) (Dutton et al., 2004). Fig. 1 showcases the damage mechanisms for the creation of BVID. As shown, the radius of damage increases through the thickness of the structure such that the impacted side of the panel exhibits very little visual indentation. Conversely, the rear of the panel visually exhibits high levels of damage. Whilst the detection of BVID on the rear of the panel can be more easily performed, limitations regarding access to this region constrain detection capabilities.

Alternative methods for detection include the development of Structural Health Monitoring (SHM) systems that are capable of real-time detection of impact events such that their source may be localized, and damage quantified. Several methods exist for the development of SHM; however, AE monitoring presents as one of the best techniques due to the strong tendency of the AE to interact with damage and its ability to propagate over large distances (Dafydd and Sharif Khodaei, 2020, Rauter and Lammering, 2015).

BVID is of particular concern in the use of FRPs as it acts as a major damage initiation source (Dutton et al., 2004, Defense., 2002). Compression forces induced during impact are carried through-thickness by the typically brittle composite matrix. Such forces initiate damage via matrix cracking that under compression loading results in delamination and the formation of sub-laminates that are prone to buckling (Wronkowicz-Katunin et al., 2019). As a result, the occurrence of BVID is often characterized by reduced flexural and compression strength of the composite. Any such damage to the FRP may likewise act as an initiation point for corrosion, reducing the life of the structure (Dutton et al., 2004).

2. Finite Element Analysis (FEA) Simulations

2.1. Setup

To inform the development of a SHM system, an explicit dynamic FEA model can be used to simulate low velocity impacts and the AEs released from such events. This work has employed the use of LS-DYNA developed by Livermore Software for such analyses. LS-DYNA is particularly well suited for the analysis of AE events in structures due to its use of the Courant-Friederich Levy (CFL) criteria that determines the time step size from the amount of time required for a stress wave – or acoustic wave - to propagate through the smallest mesh element.

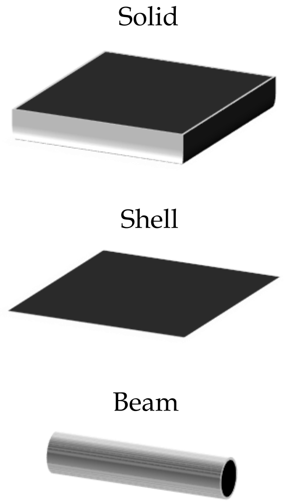

$$c = \sqrt{\frac{E(1-\nu)}{\rho(1+\nu)(1-2\nu)}}$$

$$c = \sqrt{\frac{E}{\rho(1-\nu^2)}}$$

$$c = \sqrt{\frac{E}{\rho}}$$

Fig. 2 The CFL criteria used to determine the speed of sound and time step in a variety of elements.

Whilst very useful and powerful, CFL requires intensive development of the structural mesh to ensure that the quality and total time of the simulation is well controlled. A single element of poor quality may produce an unnecessarily small time step size and hence, a very long time to solve the simulation. Likewise, by employing explicit time integration several assumptions are made that allow for generally good convergence as well as low memory requirements. Hence, LS-DYNA presents as an excellent tool for the study of highly transient events such as impact for the analysis of AEs.

Whilst the goal of this work is the development of SHM for the detection of BVID in FRPs, thus far only preliminary studies have been conducted for impacts upon an aluminium plate. Performing such preliminary studies allows for validation of the model before progressing to complex materials such as FRPs. A 10 mm diameter spherical steel projectile has been used as the impactor for a variety of impacts between 2.5 J and 20 J. The mass of the projectile is 4.11 grams, resulting in velocities for the trials as highlighted in below in Table 1.

Table 1 A summary of the impact trials

Energy (J)	Velocity (m/s)
2.50	34.88
5.00	49.32
7.50	60.41
10.0	69.76
12.5	77.99
15.0	85.43
17.5	92.28
20.0	98.65

Fig. 3 The model setup for the impact simulations on the aluminium plate.

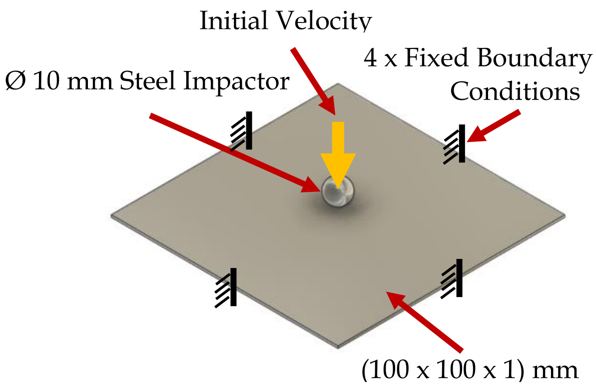

The plate has been fixed at all four edges with the projectile in the centre. A brief depiction of the simulation setup, including boundary conditions is shown in Fig. 3.

2.2. Results and Discussion

Prior to performing the impact analysis, the projectile was replaced with a simple impulse force input such that the resonance characteristics of the plate could be observed. Assessment of the resonance characteristics of the plate functions to both provide confidence in the quality of the simulation as well as a damage metric for future analysis. The results of the impulse response are shown in Fig. 4.

As evident, two resonances can be clearly observed, occurring at 85 kHz and 92 kHz. The quality of the resonant response of the plate indicates that the model has converged well. Following the impulse response, the impact trials were performed. An arbitrary node on the plate, located approximately three quarters along the diagonal from the location of impact was taken as the test location. The out-of-plane displacement or through-thickness displacement of this node was examined under the influence of the impact. As the nodal response is directly measured no analysis has been performed regarding coupling of acoustic sensors.

Fig. 4 Resonance response of the plate under an impulse.

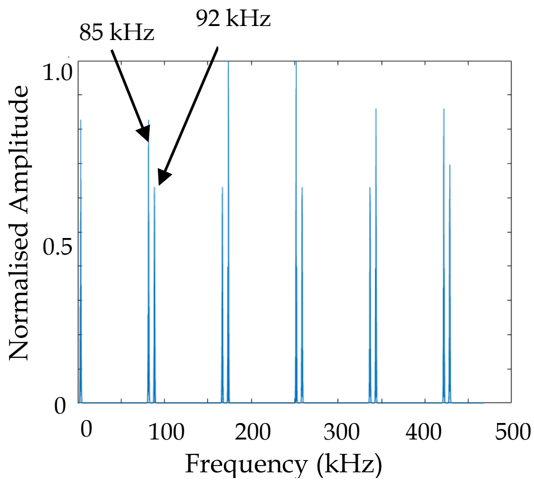

To ensure that the response of the plate under the impact was controlled for all energy levels, a two-step post-processing routine has been implemented. Firstly, as the projectile has been offset from the surface of the plate by a small distance, a time delay Δt results between each trial because of the difference in time required for the impact to occur. As such, each of the time signals have been translated to account for this Δt such that the displacement response $x(t)$ of the node is non-zero. This can be represented mathematically as follows.

$$\Delta t := x(\Delta t) \neq 0 \mid (x(t) = 0 \mid t < \Delta t) \quad (1)$$

Following this translation, the signals are detrended to remove any constant or linear displacement offsets. To accomplish this, a high-pass filter has been applied to the signals. It was observed that a cut-off frequency of 2.5 kHz worked well to detrend the signal with little warping in the response. A depiction of the time domain signals for an impact of 2.5 J and 20 J are shown in Fig. 5 following the post-processing. As can be observed, the amplitude of the response is much larger for the 20 J impact. Interrogation of the time domain AE signals as depicted can be used to localize the source of the impact. Whilst this localization has not yet been performed, methods to accomplish this are discussed in the following section.

The acquired AE signals are likewise analysed in the frequency domain as shown in Fig. 6. As can be observed, there are obvious, broadband excitations that occur at central frequencies of approximately 200 kHz and 400 kHz with frequency bands of approximately 50 kHz. Whilst there is frequency information below the 100 kHz range, the response is not well defined and would require further processing to render any useful information.

Moreover, whilst the impacts have excited the same frequency responses in the plate, the higher energy impact has resulted in stronger excitations. This behaviour is expected and hence, indicates a well-behaved model with good convergence. Finally, to showcase the modal properties of the impact as well as the permanent damage from the aluminium projectile, von Mises equivalent stress and plastic strain contour plots are shown in Fig. 7.

Fig. 5 Time domain AE signals for 2.5 J and 20 J impacts.

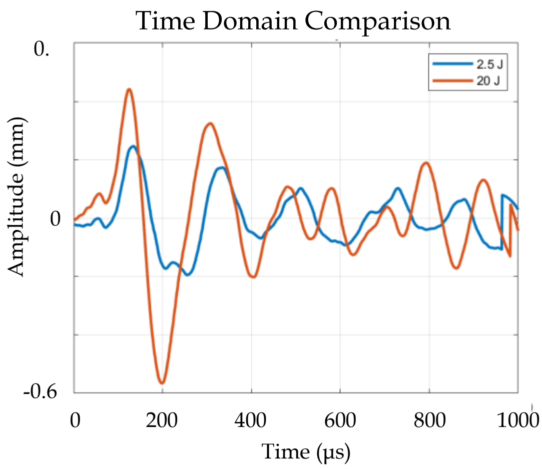

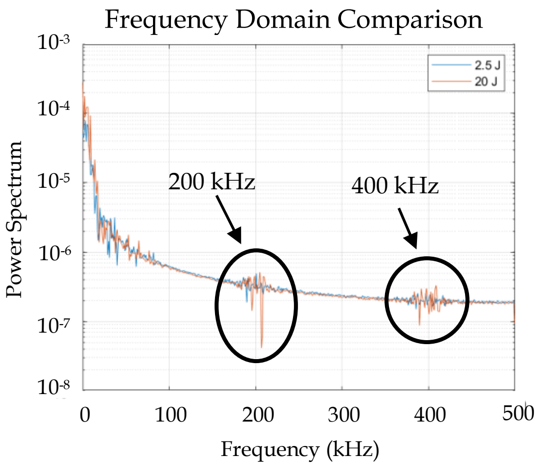

Fig. 6 Frequency domain AE signals for 2.5 J and 20 J impacts.

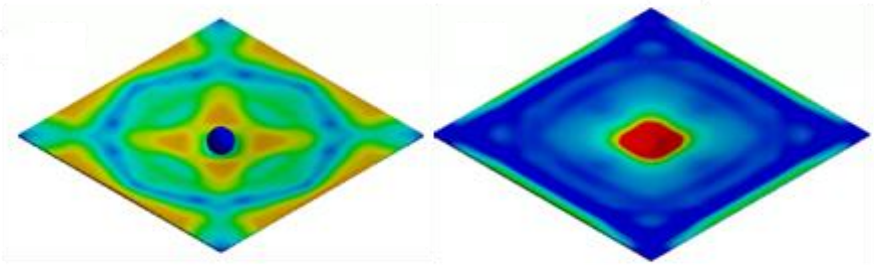

Fig. 7 von Mises equivalent stress from projectile impact and b) plastic deformation post-20 J impact.

3. Acoustic Emission (AE) Localisation

By utilising either a phased or sparse array – as shown in Fig. 7 - multiple time domain AE signals may be captured from the low velocity impacts upon the plate. There exists a variety of methods that may then be used to localize the source of the AE and hence, to localize the impact and possible location of BVID. There likewise exists the possibility of further interrogating the content of each AE to possibly yield useful information in an effort to characterize and quantify the damage event.

One such method to localize the source of the AE is through the application of a cross-correlation to calculate the time delay $\tau_{a,b}$ between adjacent sensor elements, following which a multilateration may be performed. The equations for determining the time delay and location via multilateration are shown below in Eq. 2.1 and Eq. 2.2, respectively. Methods for localization of AEs is an ongoing area of study.

$$\tau_{i,j} = \max \mathcal{F}^{-1}\left[\overline{X_a[k]} \cdot X_b[k]\right] \tag{2.1}$$

$$\tau_{i,j} c_{P_{f_0}} = \sqrt{(x_s - x_a)^2 + (y_s - y_a)^2} - \sqrt{(x_s - x_b)^2 + (y_s - y_b)^2} \tag{2.2}$$

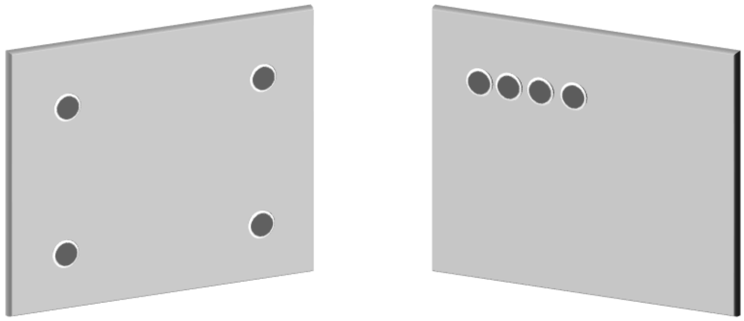

Fig. 8. Sensor configurations on a plate for a) a sparse array and b) a phased array.

X_a and X_b represent the Fourier transformation of adjacent AE signals. Likewise, $\mathcal{F}^{-1}$ is the inverse Fourier transformation and the overbar symbol denotes the complex conjugate. The phase velocity at the peak frequency component $c_{P_{f_0}}$ is used for the multilateration to determine the AE source (x_s, y_s) by knowing the location of the acquired AE signals ($x_{a/b}, y_{a/b}$). A minimum of three sensors are required to localize an AE upon a 2-dimensional plane.

4. Conclusion

Thus far, preliminary work has been conducted towards understanding the mechanics of AE propagation resulting from low velocity impacts. The results presented indicate that the proposed modelling tool of LS-DYNA has the capability to accurately depict such impact events as well as the emissions that result from them.

Work is hence being planned for the development of impacts upon FRP materials. Due to the complex damage mechanics involved with impacts upon such materials, a series of experimental tests will likewise be performed to aid in the validation of the model. Furthermore, the formation of fast and slow axes owing to the orthotropic nature of the FRP specimen will create greater difficulties in localizing the AE signal. To minimize this difficulty, the proposed specimen will use VTM 264 carbon prepreg with a quasi-isotropic layup.

References

Dafydd, I. & Sharif Khodaei, Z. 2020. Analysis of barely visible impact damage severity with ultrasonic guided Lamb waves. Structural Health Monitoring, 19, p. 1104-1122.

Defense., U. D. o. 2002. Military Handbook–MIL-HDBK-17-1F: Composite Materials Handbook, Volume 1—Polymer Matrix Composites Guidelines for Characterization of Structural Materials. US Department of Defense.

Dutton, S., Kelly, D. & Baker, A. 2004. Composite materials for aircraft structures, American Institute of Aeronautics and Astronautics.

Fawcett, A. J. & Oakes, G. D. Boeing composite airframe damage tolerance and service experience. Composite damage tolerance & maintenance workshop, 2006. p.

Kumar, P. & Rai, B. 1993. Delaminations of barely visible impact damage in CFRP laminates. Composite Structures, 23, p. 313-318.

Mustapha, S., Ye, L., Dong, X. & Alamdari, M. M. 2016. Evaluation of barely visible indentation damage (BVID) in CF/EP sandwich composites using guided wave signals. Mechanical Systems and Signal Processing, 76, p. 497-517.

Rauter, N. & Lammering, R. 2015. Impact damage detection in composite structures considering nonlinear lamb wave propagation. Mechanics of Advanced Materials and Structures, 22, p. 44-51.

Saeedifar, M., Najafabadi, M. A., Zarouchas, D., Toudeshky, H. H. & Jalalvand, M. 2018. Barely visible impact damage assessment in laminated composites using acoustic emission. Composites Part B: Engineering, 152, p. 180-192.

Wronkowicz-Katunin, A., Katunin, A. & Dragan, K. 2019. Reconstruction of barely visible impact damage in composite structures based on non-destructive evaluation results. Sensors, 19, p. 4629.